We are IntechOpen,
the world's leading publisher of Open Access books
Built by scientists, for scientists

4,800
Open access books available

122,000
International authors and editors

135M
Downloads

Our authors are among the

154
Countries delivered to

TOP 1%
most cited scientists

12.2%
Contributors from top 500 universities

CLARIVATE ANALYTICS
BOOK CITATION INDEX
INDEXED

WEB OF SCIENCE™

Selection of our books indexed in the Book Citation Index
in Web of Science™ Core Collection (BKCI)

Interested in publishing with us?
Contact book.department@intechopen.com

Numbers displayed above are based on latest data collected.
For more information visit www.intechopen.com

Backbone Connectivity and Collective Aggregation Phenomena in Polymer Systems

Wen-Jong Ma[1,2] and Chin-Kun Hu[2]
[1]*Graduate Institute of Applied Physics, National Chengchi University,*
Taipei 11605
[2]*Institute of Physics, Academia Sinica, Nankang, Taipei 11529*
Taiwan

1. Introduction

A convenient theoretical entry to tackle the protein aggregation problems is to track on the origin of the aggregation phenomena from the viewpoint of polymer physics, enquiring how the underlying factors, such as the geometric packing, the topology and their mutual interplays in presence of solvent, play their roles in the processes. Such a view has been inspired by recent experiments [1, 2] and molecular dynamics simulations [3, 4] which suggest the ubiquitous presence of fibril formation [5] in various natural and laboratory prepared proteins or peptides. While the variety of amino acid sequences interferes with the occurrence of long-range structural ordering, a material-insensitive tendency of aggregation is observed [2, 3, 5]. By coarsening the sequence-sensitive details, the aggregation problem can be formulated in its minimal form as the clustering process of polymer chains [6, 7]. With such simplified models, the approach focuses more on the entropic effect caused by the constraint of chain connectivity [6–8], rather than on the material-dependent characteristics. In this chapter, we summarize our molecular dynamics simulation studies [6, 7] that reveal the relationship between the backbone connectivity of polymer chains and some benchmark features displayed in the aggregation processes of the model polymer chains.

In the model, the backbone connectivity of a polymer chain is realized by assigning a string of monomers with specific monomer-monomer two-body forces, perturbed with three-body and four-body angle dependent interactions [6], with their strengths measured by the parameters, k_{nn}, K_b and K_t, for the nearest neighbor (n.n.) interaction, the bending angle and the torsion angle potentials, respectively. In a collection of polymer chains, all the non n.n. pairs along a chain and those pairs on different chains are subject to Lennard-Jones (L-J) pair interactions. The presence of angle potentials, with significantly nonzero K_b or K_t values, breaks the isotropy surround the backbone. In such a system, the local inter-chain hindrance prevents the chains from clustering into ordered domains. The situation can, however, be reverted by reducing the values of K_b and K_t. We find that the formation of bundle-like domains (Fig. 1) is robust as soon as K_b and K_t are small enough. The observations are assured even if we introduce a small amount of dispelling background fluid molecules or impose a small fraction of impurity monomer sites.
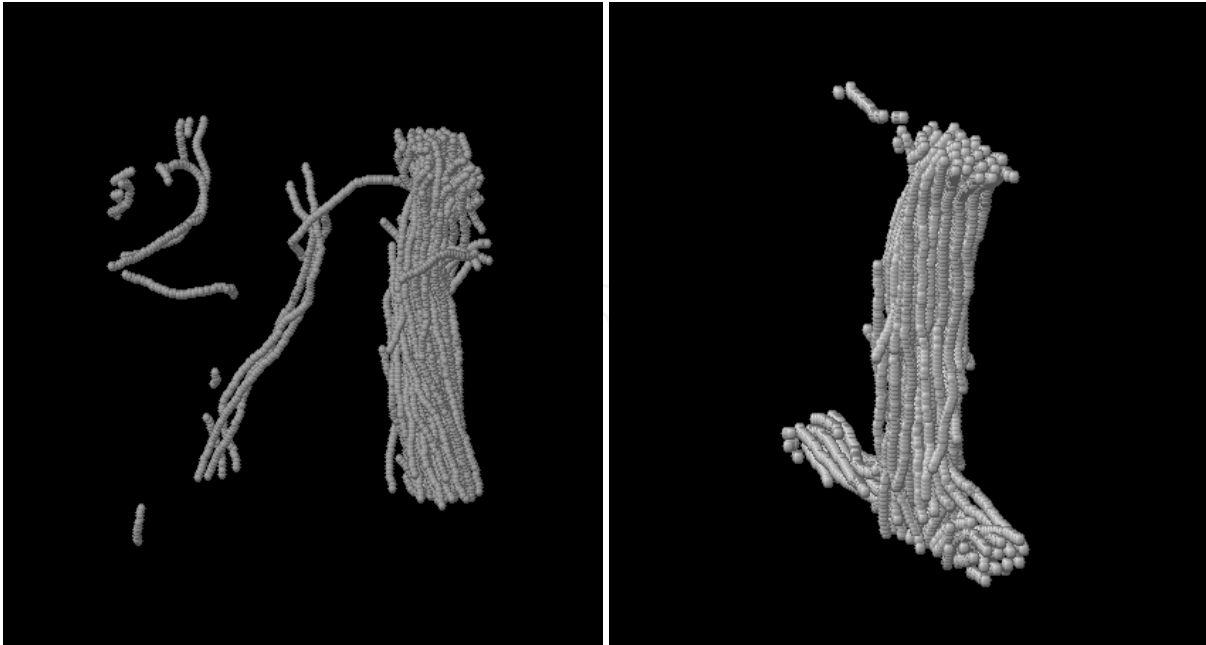
Fig. 1. Bundled domains formed in systems of homopolymer chains, with zero (left plot) or tiny (right plot) values in K_b and K_t. They are snapshots for the systems with rigid bonds, labeled by I-∞ and III, respectively, in Table 1.

In quantifying the overall structural changes over the relaxation processes, we reveal the shared scenario for the cluster forming procedure in a range of systems (see Table 1) . In this scenario, the ordering of the clustered (bundled) domains can occur spontaneously as soon as the energy barriers contributed by the local structural hindrance are overcome. Under such circumstances, the completion of aggregation always occurs at a temperature well above the characteristic temperature determined by the strength ϵ of the site-site L-J pair potential. This is in contrast to the formation of ordered clusters in the two phase coexistence region for a L-J fluid of the same number of monomers. (The system is equivalently obtained by removing those n.n. bonding along the polymer chains.) The clustering can only occur below the critical point temperature, which is about 1.3 times of the characteristic temperature ϵ/k_B (k_B: Boltzmann constant). To have solid-like structured cluster, the temperature has to go below the triple point temperature, which is about $0.6\epsilon/k_B$. The result suggests that the key role played by the chain connectivity is via the lowering of the entropy of the system, so that the formation of ordered domains, becomes feasible at a temperature not necessarily very low for the system to overcome the local structural hindrance.

The bonding strength, parameterized by k_{nn}, of the nearest neighboring monomers along the chains affects the detailed procedures in the formation of clusters during the aggregation processes. More than one stages are present during the processes, with the local alignment of segments in the individual chains followed by the coalescence of these short patches. The second stage is found further to differentiate into several stages with the increased k_{nn}. We allow k_{nn} to have infinity value, which is realized in simulation as a (rigid) bond with fixed length maintained by the constraint force (see Section 2.1). In manipulating the parameters k_{nn}, K_b and K_t in a range of systems, we can obtain more precise information about how the backbone anisotropy prevent the polymer chains from the formation of bundled structure. The scenario unveiled in this study may be useful for the analysis of protein aggregation phenomena in realistic complex biological systems.

system	label	N_P (# chain)	n (# monomer per chain)	N_F (# fluid atom)	k_{nn} (n.n. strength)	K_b (bending angle strength)	K_t (torsion angle strength)
set I‡	I-1	40	100	0	10	0	0
	I-2	40	100	0	10^2	0	0
	I-3	40	100	0	10^3	0	0
	I-4	40	100	0	10^4	0	0
	I-4	40	100	0	10^4	0	0
	I-∞	40	100	0	∞	0	0
	I-A	80	50	0	∞	0	0
	I-B	160	25	0	∞	0	0
set II§	II-0	40	100	6000	1	10^{-4}	10^{-4}
	II-1	40	100	6000	10	10^{-4}	10^{-4}
	II-2	40	100	6000	10^2	10^{-4}	10^{-4}
	II-3	40	100	6000	10^3	10^{-4}	10^{-4}
	II-4	40	100	6000	10^4	10^{-4}	10^{-4}
	II-∞	40	100	6000	∞	10^{-4}	10^{-4}
set III♮	III	40	100	0	∞	10^{-4}	10^{-4}
set IV†	IV-0	40	100	6000	1	0.1	0.1
	IV-1	40	100	6000	10	0.1	0.1
	IV-2	40	100	6000	10^2	0.1	0.1
	IV-3	40	100	6000	10^3	0.1	0.1
	IV-4	40	100	6000	10^4	0.1	0.1
	IV-∞	40	100	6000	∞	0.1	0.1

Table 1. List of systems
‡ systems of pure isotropic ($K_b = K_t = 0$) homopolymer chains (see Ref.[6, 7]);
§ systems of chains with tiny backbone anisotropy ($K_b = K_t = 10^{-4}$) and with ≈ 5% (199 out of nN_P =4000) impurity monomers (see Ref.[6, 7]), mixed with fluid atoms ($N_F > 0$) ;
♮ a pure system of rigidly bonded homopolymer chains with tiny backbone anisotropy and without impurity monomers (see Ref.[7]);
† systems of anisotropic ($K_b = K_t = 0.1$) chains that fail to aggregate; there being ≈ 5% (199 out of nN_P =4000) impurity monomers (see Ref.[6, 7]) and mixing with fluid atoms ($N_F > 0$).

2. Model and analysis

2.1 Model systems

nearest neighbor bonding

We consider systems containing $N_P = 40$ polymer chains and each chain has $n = 100$ monomers. Two major sets of systems are studied. The first set (set I) are pure ($N_F = 0$) systems of homopolymer chains with no built-in anisotropy with respect to the backbone ($K_b = K_t = 0$), which can be classified phenomenologically as a bead-spring (if $k_{nn} < \infty$) or a bead-rod (if $k_{nn} = \infty$) model [9, 10]. The nearest neighbors i and j at a distance r_{ij} in our bead-spring chains are connected by the potential
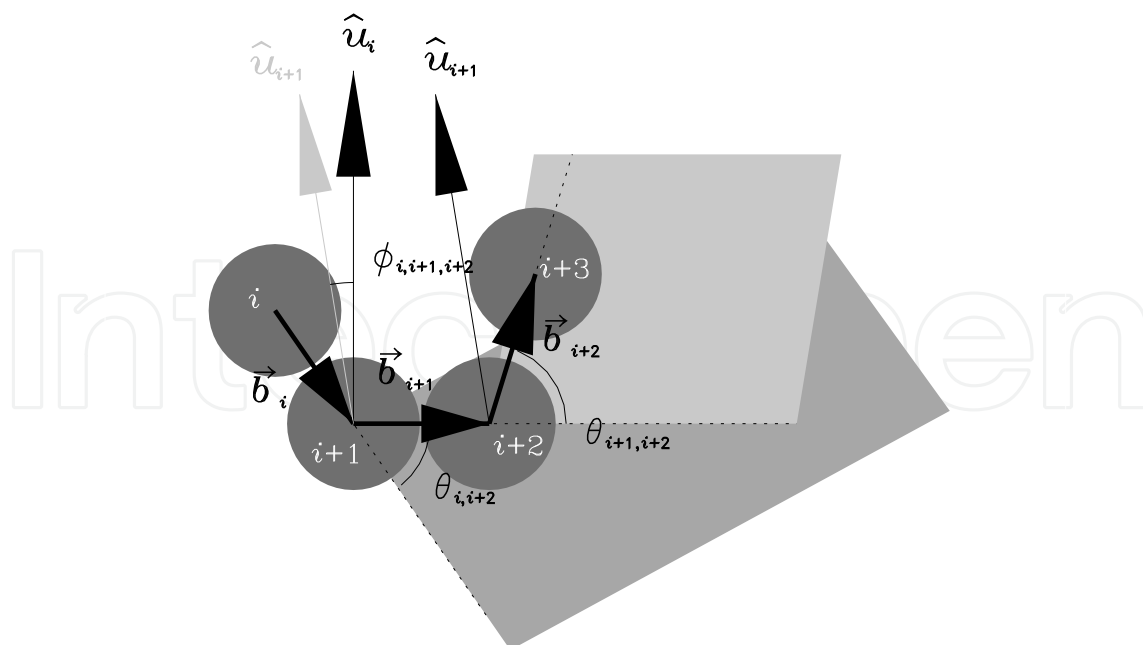
$$V_s(r_{ij}) = \frac{1}{2}k_s(r_{ij} - r_0)^2$$

Fig. 2. Bending angle $\theta_{i,j,k}$ and torsion angle ϕ_{ijkl} extended by the consecutive monomers i, $j = i + 1$, $k = i + 2$ and $l = i + 3$ along a chain.

with its strength constant k_s, the $k_{nn} = 10^s$ multiple of the value k_0 (i.e. $k_s = k_{nn}k_0$) and balance length r_0, for the five systems with $s = 1, 2, 3, 4$ (k_0 and r_0 are given below). They are labelled as I-s (I-1, ..,I-4, etc) systems in Table 1. The bead-rod chains in our model are chains with strict constant nearest neighbor bond lengths and are realized numerically by Lagrange's constraint forces using RATTLE numerical scheme [11]. The system is labelled as system I-∞ in Table 1.

In all these model systems, the pair interactions between the non-neighboring monomers along a chain or between pairs in different molecules, i and j at a separation r_{ij}, are L-J potentials

$$V_{LJ}(r_{ij}) = 4\epsilon((r_{ij}/\sigma)^{-12} - (r_{ij}/\sigma)^{-6}).$$

In terms of the distance parameter σ and the strength parameter ϵ of L-J potential, we choose $k_0 = 1.5552 \times 10^5 \epsilon\sigma^{-2}$ and $r_0 = 0.357\sigma$ [6, 12].

backbone anisotropy along the chains

In the second set (set II) of systems, the degrees of backbone anisotropy along the chains are introduced by perturbing bending potential,

$$\Theta(\theta_{i,j,k}) = K_b c_b (cos\theta_{ijk} - cos\theta_0)^2,$$

determined by the bending angle $\theta_{i,j,k}$ of three consecutive monomers i, j and k along a chain; and the torsion potential [13]

$$\Phi(\phi_{ijkl}) = K_t \sum_{\iota=0}^{3} a_\iota (cos\phi_{i,j,k,l})^\iota$$

as a function of the torsion angle ϕ_{ijkl} extended by four consecutive monomers i, j, k and l (see Fig. 2). The constants c_b, θ_0 [12]; and a_1, a_2 and a_3 [13] are given so that a model polyethelyne
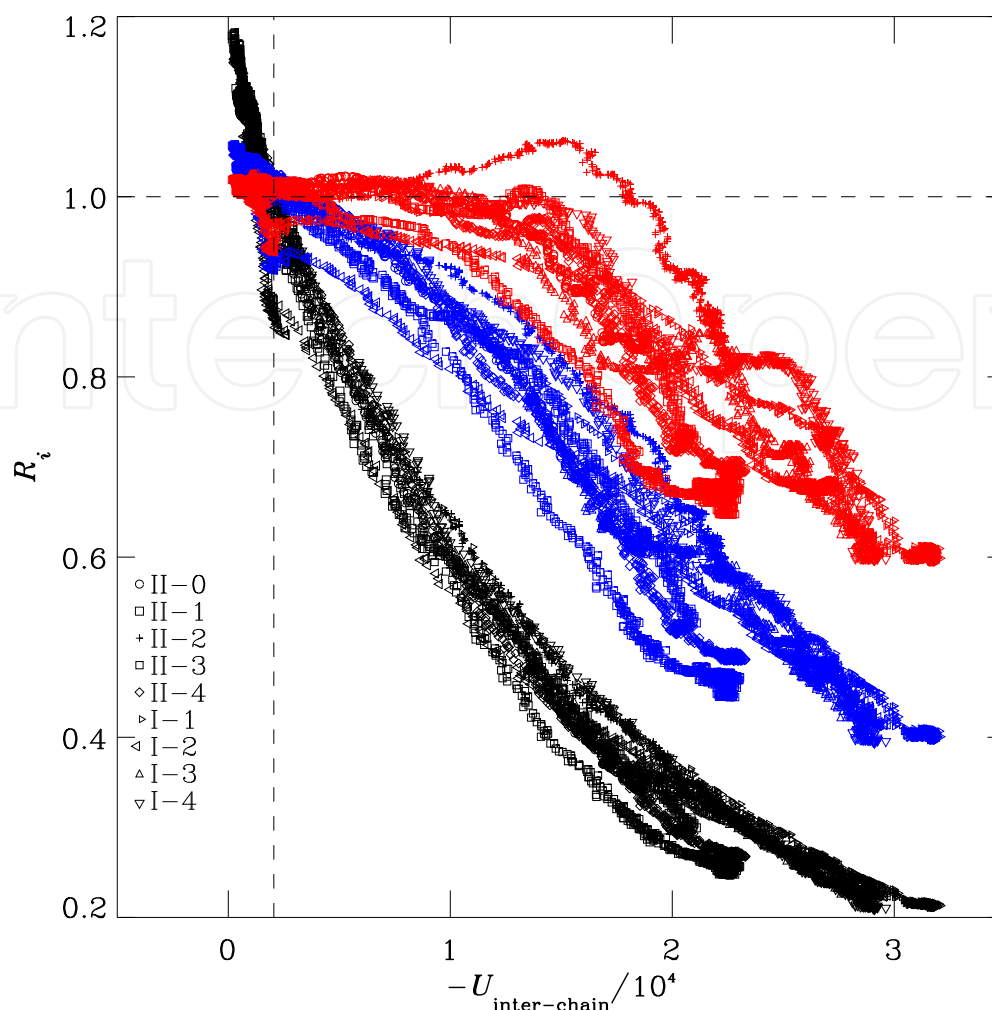
Fig. 3. R_0 (black), R_1 (blue) and R_2 (red) versus $-U_{\text{inter}-\text{chain}}$, for systems set I: I-1, I-2, I-3, I-4 and set II: II-0, II-1, II-2, II-3 and II-4, which contain chains with their nearest neighbor connected by spring forces (see Table 1).

chain is obtained by choosing $r_0 = 0.357\sigma$, and let the strength control parameters K_b and K_t be unity [12, 14]. With a range of values for K_b and K_t and a choice of bending angle parameter θ_0, we are able to prepare chains with different degrees of local conformational hindrance [6, 15]. In our simulations, we prepare several systems, each composed of identical chains with $K_b = K_t$, which are allowed to have the value 0, 10^{-4} or 0.1 (see Table 1). The model mimics qualitatively the dispersed local conformational degrees of freedom that is present in those structured monomers, such as the amino-acids in protein molecules.

For systems in set II, the chains is further perturbed by randomly imposing a fraction of 5% monomers to have smaller sizes. In merging with monomer-repelling Lennard-Jones fluid atoms, the heterogeneity is further enhanced by rendering these 5% monomers to interact, in addition to the repulsive force, with an attractive part with the fluid atoms [6, 7]. Under the convention mentioned above, we label those systems as II-s ($s = 0, 1, 2, 3, 4$ or ∞) in Table 1, according to the exponent of the multiple ($k_{\text{nn}} = 10^s$ or ∞) of their nearest bonding strength $k_s = k_{\text{nn}}k_0$.

Three additional systems of pure ($N_F = 0$) homogeneous rigidly-bonded chains are also studied. Two of them that contain the same rigidly bonded chains, of shorter chain lengths
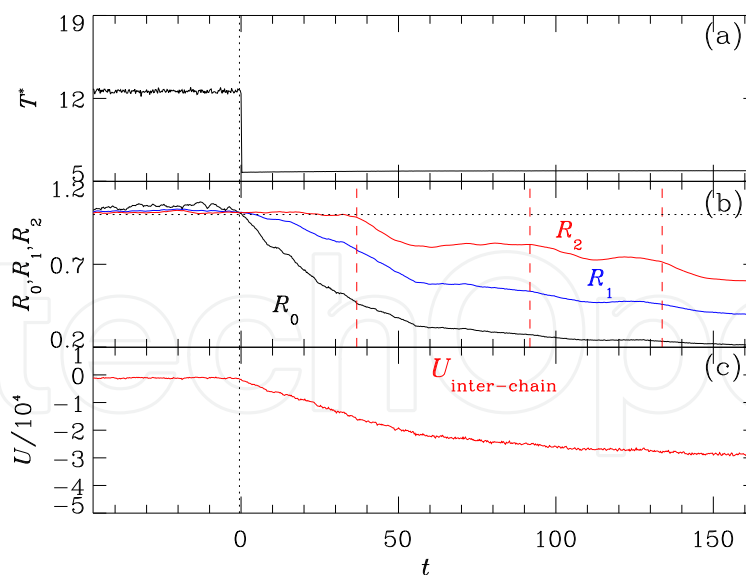
Fig. 4. Time evolutions of (a) instantaneous temperature T^*; (b) the parameters R_0 (solid line), R_1 (dash dot line) and R_2 (dashed line); and (c) the inter-chain potential energy, for system I-4 (adapted from Ref. [6]).

($n = 25$ and $n = 50$, respectively), are included in set I. They are used to underscore the effect of chain length. The other system consists of homopolymer chains to have the same backbone anisotropy ($K_b > 0$ and $K_t > 0$) as those in set II, but in absence of the 5% impurity monomers. We list this system as system III. Table I lists all the systems that are analyzed in this chapter. Each of them contains the same number $nN_p = 4000$ of monomers.

To show that the increased backbone anisotropy indeed hinders the ability to aggregate, we list the systems set IV in Table 1, which are different from their counterparts in set II, only in the 1000 times larger values in K_b and K_t (=0.1).

quenching

According to the scenario of clustering, the polymer chains aggregate when the temperature and the density of the systems fall within the coexistence region of the phase diagram. In the systems of polymer chains with rigid bonds, a quenching can be achieved by the numerical effect for the cases $K_b = K_t \leq 10^{-4}$, that a convergence to satisfy holonomic constraints on bond lengths lead the dynamic system toward the low temperature attractor [7]. The system is, therefore, quenched spontaneously. With the bond constraints replaced by the confining of soft interaction potentials, on the other hand, the incoherence among the springs in different bonds does not favor a global numerical convergence. In order to lower the temperature of the polymer chains in this case, we have to control the simulated system manually by using a thermostat.

Since the distributions of the monomer velocities are known to deviate systematically from the standard Maxwell-Boltzmann with the increased strength of nearest neighbor bonding [16, 17] and are described by the Tsallis q-statistics [18], if the system reaches a "quasi-steady state", it is inappropriate to use the existing thermostating methods that would force the simulated system to converge to a state described by standard Maxwell-Boltzmann statistics. A naive choice without imposing presumed statistics is simply controlling *only* the mean value of the kinetic distributions. In the simplest version of the "velocity scaling" thermostat [19], we
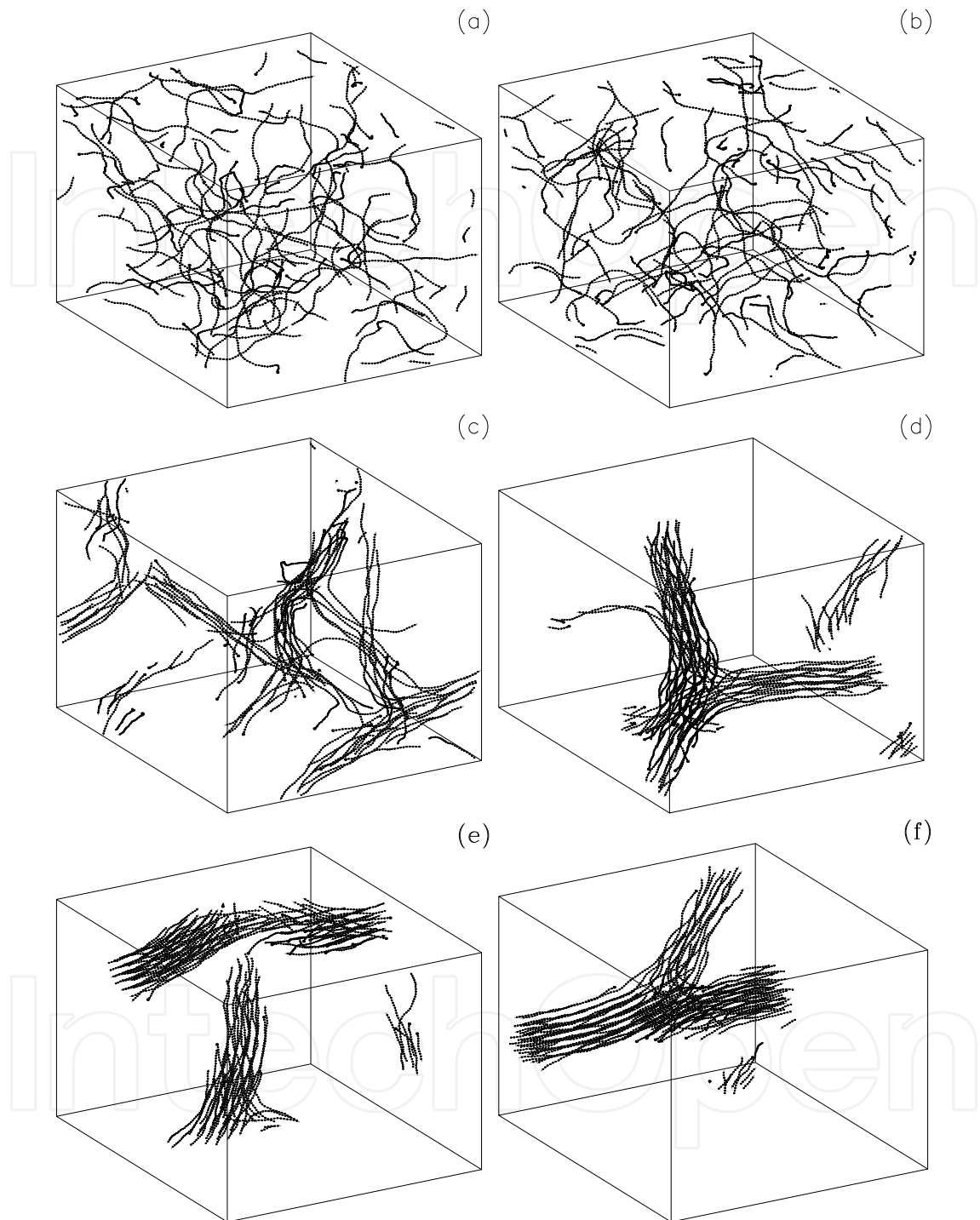
Fig. 5. Snapshots of the configurations of system I-4, for the process described by Fig. 4, in the pure system ($K_b = K_t = 0$) with $k_{\mathrm{spring}} = k_4$, (a) before ($t$=-47, the starting time in Fig. 4) and (b) on the initiation of aggregation ($t = 0$); (c), (d), and (e), respectively, at the onset step of the first, the second and the third fast decaying for R_2 (the time spots of which are marked by vertical lines in Fig. 4(b)); (f) the last step in Fig. 4 (adapted from Ref. [6]).
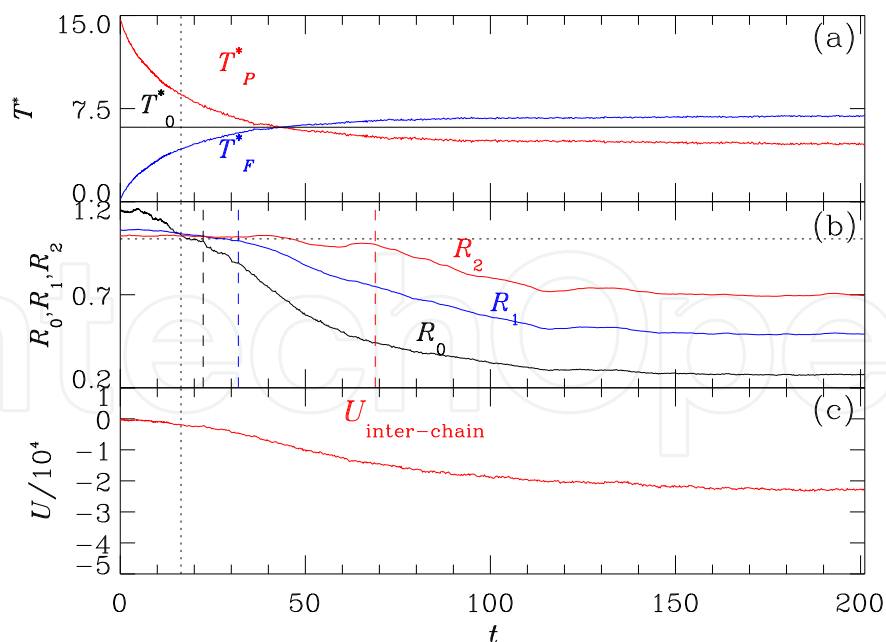
Fig. 6. Same as Fig. 4, for system II-4, which has tiny values for $K_b = K_t = 10^{-4}$. (adapted from Ref. [6]).

re-scale the velocities of the monomers and the L-J molecules at *every* step by a factor forcing the mean kinetic energy for the *whole* system to the value of the target temperature T_0^*.

2.2 Parameters to identify clustering

To quantify the overall structural change of the simulated systems over their non-equilibrium relaxation processes, we define the following parameters. For a system of N_P polymer chains each with n monomers in a simulation cubic box of size $L \times L \times L$ subject to periodic boundary conditions, we use the parameters [7]

$$R_k \equiv \frac{\int_0^{\frac{L}{2}} g_{\text{interchain}}(r) r^k dr}{\int_0^{\frac{L}{2}} \Xi(g_{\text{interchain}}(r)) r^k dr} \tag{1}$$

for $k = 0, 1, 2$, to monitor the degree of clustering, where $\Xi(x) = 1$ if $x \neq 0$ and $\Xi(x) = 0$ if $x = 0$. The parameters are evaluated by finding the interchain pair distribution function $g_{\text{interchain}}(r)$, which is defined as

$$g_{\text{interchain}}(r) 4\pi r^2 dr = \frac{1}{N_m} \sum_{i=1}^{N_m} \{ \frac{V}{N_m - n}$$
$$\times \sum_{\substack{j(i \text{ and } j \text{ in different chains}) \\ r < r' \leq r + dr}} \delta(|\vec{r}_{ij}| - r') \} \tag{2}$$

for $r < L/2$, where $N_m = nN_P$ is the total number of monomers. R_0, R_1 and R_2 provide information about the conformational features of the clusters at different stages of the growth process. In particular, the condition for uniformly distributed situation, $R_0 = R_1 = R_2 = 1$ can be used as a criteria to locate the time spot of initiation of the aggregation process when such a condition starts to become untrue.
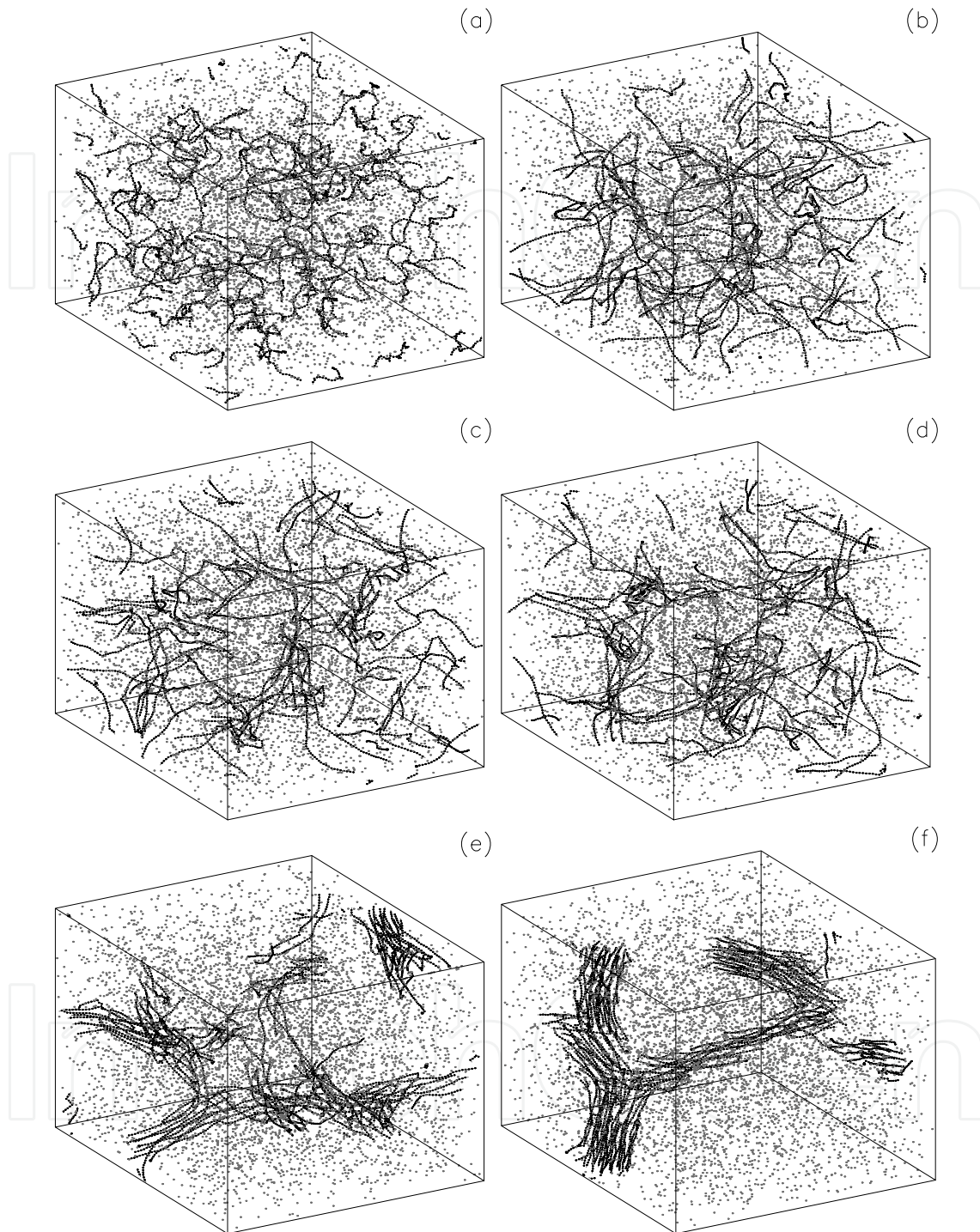
Fig. 7. Snapshots of the configurations for the aggregation process in system II-4, i.e. the mixed system with $K_b = K_t = 1.0 \times 10^{-4}$ and $k_{spring} = k_4$, at (a) t=0; (b) the initiation of aggregation ($R_0 \approx R_1 \approx R_2 \approx 1$); the onset step of fast decaying of (c) R_0, (d) R_1 and (e) R_2; (f) the last step of Fig. 6. The time spots for (c), (d) and (e) are marked by vertical lines in Fig. 6(b) (adapted from Ref. [6]).

The formation of clusters can be identified by the trend to have the lowered total interchain (L-J) potential energy $U_{interchain}$ and a decreasing virial $v_{interchain}$ (see Ref. [7]). Since both $v_{interchain}$ and $U_{interchain}$ follow the same trend [6, 7] and the latter is subject to much less fluctuations than the former is, we adapt here $U_{interchain}$ as the major quantity to monitor the process.

3. Aggregation of polymer chains

3.1 Stages of the clustering process

The formation of clusters can be identified by the tendency to have lowered total interchain (L-J) potential energy $U_{interchain}$. Figure 3 shows the parameters R_0, R_1 and R_2 decrease as the functions of $U_{interchain}$, over the dynamic relaxation processes for the nine systems with soft n.n. bonding ($k_{nn} < \infty$), for either pure homopolymer chains (N_F=0 and $K_b = K_t = 0$, i.e. systems I-1, I-2, I-3 and I-4) or mixed heterogeneous chains with backbone anisotropy ($N_F > 0$ and $K_b > 0$ or $K_t > 0$, i.e. systems II-0, II-1, II-2, II-3 and II-4) listed in Table 1. The data are collected in equal time intervals [6, 7]. The increasing of the quantity '$-U_{inter-chain}$', which is used as the variable for the horizontal axis, corresponds to the direction for the growth of clusters. The parameter R_0 decreases, more or less, smoothly and is concave upward for all systems before reaching the tail regimes with densely accumulated data points, when the size of the clusters virtually saturate under the given temperature and the space constraint by the simulation box. The parameters R_1 and R_2, on the other hand, show the reflected s-shaped decreasing curves before entering the same stalled growth regimes. The reflections in the curves of R_2 are so strong that overall the shapes are close to the letter "z".

The parameter R_0 reflects the increasing contact between the pairs of monomers in different chains during the relaxation processes, over which the line geometry of the chains governs the values. The parameters R_1 and R_2, on the other hand, contain information about the clustering of higher order structures. The three parameters meet at $R_0 = R_1 = R_2 = 1$, corresponding to a spatially uniformly distributed configuration. In simulation, it can be taken as a criteria to find the time spot of initiation of an aggregation process. By the same token, the reflection points in R_1 and R_2 can be identified to divide the processes into stages of growth.

Figure 4 shows the time evolution of a typical process of aggregation in a pure homopolymer system (I-4). The temperature of the system is controlled with a target temperature $T_0^* = 6$, starting from $t = 0$. We can identify the presence of multi-stage plateaus in the subsequent process.

To refine an aggregation process into a number of stages of relaxation, we identify each time spot at which the value of one of the parameters R_0, R_1 or R_2, starts to fall rapidly at the end of each plateau. In general, while the time spot of the triggered rapid decay in R_0 may not be distinguishable from the initiation time (at which R_0=R_1=R_2=1), the onset of the fast falling in the value of R_1 and, especially, that of R_2 can easily be identified. The latter signals the growth transverse to the backbone. The chains in the system I-4 described in Fig. 4 have the stiffest springs among the spring bonded systems in set I (Table 1). The clustering process would become stuck and the system would need to wait until the initiation of the next major growth before there is another rapid fall in the value of R_2. In Fig. 4(b), the fast decaying for both R_0 and R_1 start at $t = 0$. Such time spots for R_2 can be identified (marked by dashed lines) for three sections of plateaus, at $t = 36.75$, 91.75 and 133.75, respectively. The snapshots at these time spots, together with those at the beginning and the ending of the time span plotted in Fig. 4, are shown in Fig. 5.

3.2 Backbone anisotropy and spring stiffness

The process for a mixed system (system II-4) of polymer chains, with perturbed backbone anisotropy ($K_b = K_t = 10^{-4}$) and impurity monomers, shows similar features (Fig. 6) as those found in system I-4 (Fig. 4). While the chains possess the same strengths in the monomer-monomer bonding springs as those in system I-4, the time evolution in Fig. 6(b) seems to show less tendency to become stuck over the relaxation process, as compared with its counterpart in Fig. 4(b). The corresponding snapshots of those time spots at the onsets of the fast decaying in R_0, R_1 or R_2 are shown in Fig. 7.

A quantitative comparison between the configurations at the onsets of the rapid decaying in R_2 for system I-4 (Fig. 5(c)) and II-4 (Fig. 7(e)) is carried out by plotting the full monomer-monomer pair distribution functions $g(r)$ in Fig. 8. To underscore the effect of the strength of the springs, we also put the data for the configuration at onset of R_2 for system II-0, which is a mixture system having the softest spring bonding in set II listed in Table 1. Each function $g(r)$ shows a power-law like decaying curve in increasing r (see the log-log plot in the inset of Fig. 8), until reaching a minimum, which corresponds to the void regions next to the crowded domains of clusters. The thickness of the segments of the aggregated bundles can be estimated by locating r for such a minimum in $g(r)$. While the two mixed systems (II-0 and II-4, marked by "A" and "B" respectively) have about the same bundle thickness, the packing in each system has its dependence on the strength of the monomer-monomer connecting springs. The plot shows the packing for chains in system II-0 has a crossover (the curve in the inset of Fig. 8), in contrast to the single power-law like behavior for those connected by strong springs (system II-4). The comparison between the data for system I-4 and II-4 indicates that the bundles formed in the pure polymer system (I-4, marked by "C")) is more compact than its counterpart in the mixed system (II-4, marked by "B"). The onset of the (first) fast growing stage requires larger size subunits in the mixed system with backbone anisotropy than those in the isotropic pure system.

Figure 9 shows the R_i parameters versus $U_{\text{interchain}}$ for the three cases with monomers connected by rigid bonds, $k_{nn} = \infty$ (system I-∞, system II-∞ and system III), listed in Table 1. The curves share the same qualitative features as those in Fig. 3. A quantitative comparison of the curves for R_0 shows the larger degree of curving for systems with rigid bonding than the cases with soft bonding, as a result of less flexible patching among packed chains.

3.3 Chain length dependence

For the two pure homopolymer systems ($N_F = 0$) with isotropic ($K_b = K_t = 0$) rigidly bonded ($k_{nn} = \infty$) chains (systems I-A, $n = 50$ and I-B $n = 25$, in Table 1), each containing the same total number of monomers (nN_p=4000), there are two major aggregated clusters in each case. The clusters have bundled structures and are tilted from the axes of simulation boxes, which suggest the independence of the boundary conditions in the formation of bundles. On a close examination of the snapshots of the structures (Fig. 10), we find that the effects of close sphere-packing lead to the tendency to deviate from a parallel bundled structure and lead to the formation of spiral-like local ordering (left plot of Fig. 10). Such orderings cannot, however, extend to the whole chain as the length of the chain becomes larger (middle and right plots of Fig. 10). In Fig. 11, we compare the monomer-monomer pair distributions among the three cases $n = 25$, $n = 50$ and $n = 100$. The humps behind the sharp, delta-function-like peaks, signal the ordering of sphere-packing. They are apparently larger for $n = 25$ and $n = 50$ than those for $n = 100$. The new ordering, other than that imposed by chain connectivity, is stronger for short chains.
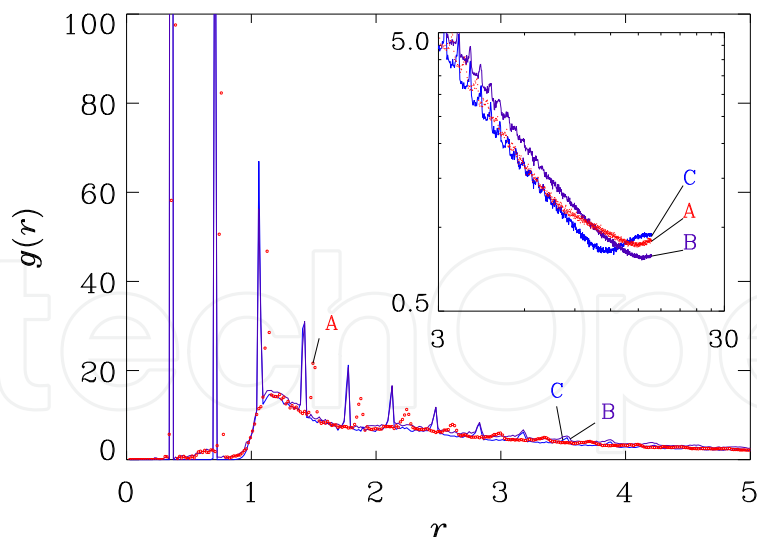
Fig. 8. (Color online) Monomer-monomer pair distribution functions for configurations in the systems II-0 (dots labeled as "A"), II-4 (solid line labeled as "B") and I-4 (solid line labeled as "C") at the onset time for fast falling R_2. The inset shows the data in log-log plot (adapted from Ref. [6]).
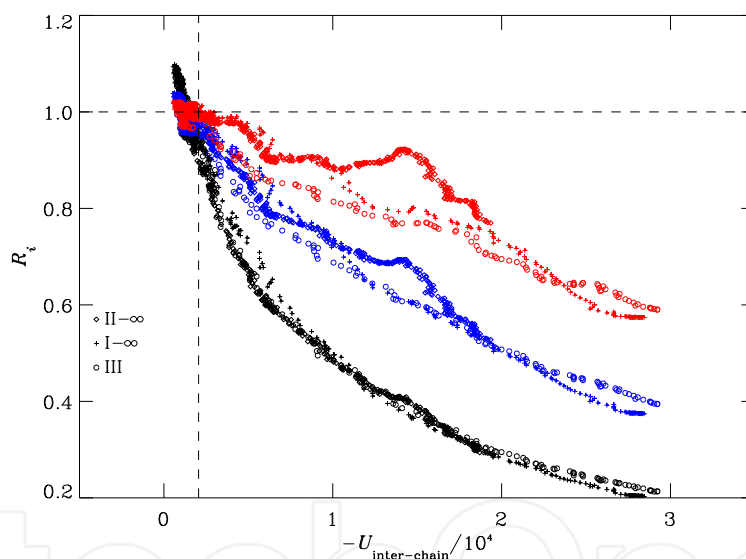

Fig. 9. Same as Fig. 3 for systems of rigidly-bonded chains.

An examination on the time evolutions (Fig 12 and Fig. 13) in these two systems, I-A and I-B, show also corresponding dynamic effects. Since the parameters R_0, R_1 and R_2 feature the line-like, plane-like, and volume-like packed spatial structures, respectively, the returning of R_2 to a larger value in the later stage of evolution indicates the prevailing of three dimensional packing. The latter trend results in the larger values in volume. Figure 14 shows the R_0 and R_1 for $n = 25$ and $n = 50$ follow the decreasing trend in the growth processes, corresponding to reducing $U_{\text{inter-chain}}$ (or increasing $-U_{\text{inter-chain}}$) which is the same as those for systems of longer chains (the cases of $n = 100$ in Figs. 3 and 9), in contrast to the returning of R_2 to a larger value in the later stage. The latter trend is stronger for the shorter chains. The result strongly suggests the relevance of chain length on the structural formation in aggregation phenomena.
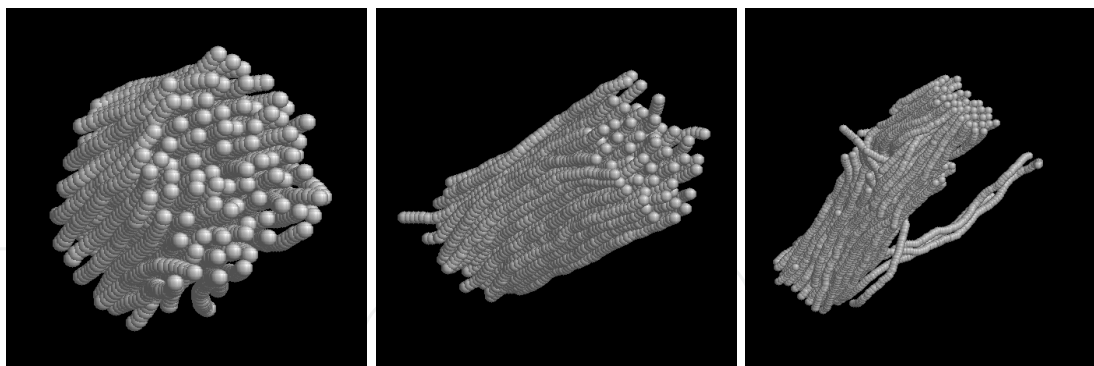
Fig. 10. Snapshots of the largest aggregated clusters for (left plot) $n = 25$, consisting of 81 chains, for (middle plot) $n = 50$), consisting of 51 chains, and for (right plot) $n = 100$, consisting of all 40 chains of the systems (adapted from Ref. [7]).
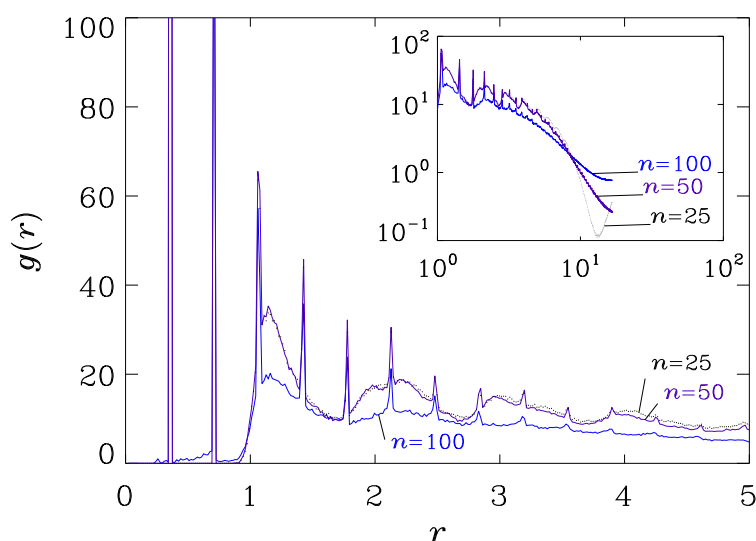

Fig. 11. (Color online) Comparison of monomer-monomer pair distributions of the aggregated configuration for $n = 25$ (blue line), $n = 50$ (red line) and $n = 100$ (black line) (adapted from Ref. [7]).

4. Growth hindered by backbone anisotropy

We have compared the aggregated structures between the systems with zero (system I-4) and with non-zero, but tiny angle potentials (system II-4),. While they both possess bundled clusters (Fig. 1), the non-zero tiny angle potentials break the symmetry to have a branched structure (right plot of Fig. 1). One more sensible question to solve is to ask if the bundled cluster can survive under even larger strengths in angle potentials. The simulations with chains having $K_b = K_t = 0.1$ (set IV in Table 1), which is 1000 times larger than those of the systems in set II have shown no cluster domains formed over time spans equivalent to or larger than those considered for systems in set II [6, 7]. The systems are brought to states at lower temperatures in a stepwise manner, with decreasing target temperature T_0^* at 8, 6 and 3, respectively, in three stages. We do observe the formation of local parallel conformations. But this local ordering can hardly extend to either the larger segment or to the gathering of more chains. The results indicate that the effect of frustration between the straight bundled packing and the local curvature imposed by the angle potentials prevent the aggregation. Such an observation is suggestive in considering more complicated material systems.
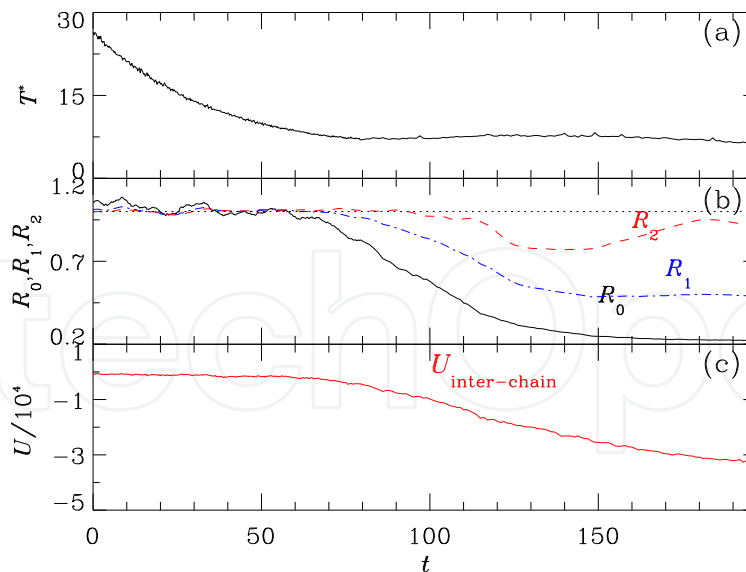
Fig. 12. Same as Fig. 4, for a simulated system with rigidly bonded homogeneous chains ($k_{nn} = \infty$) of length $n = 50$ each (adapted from Ref. [7]).
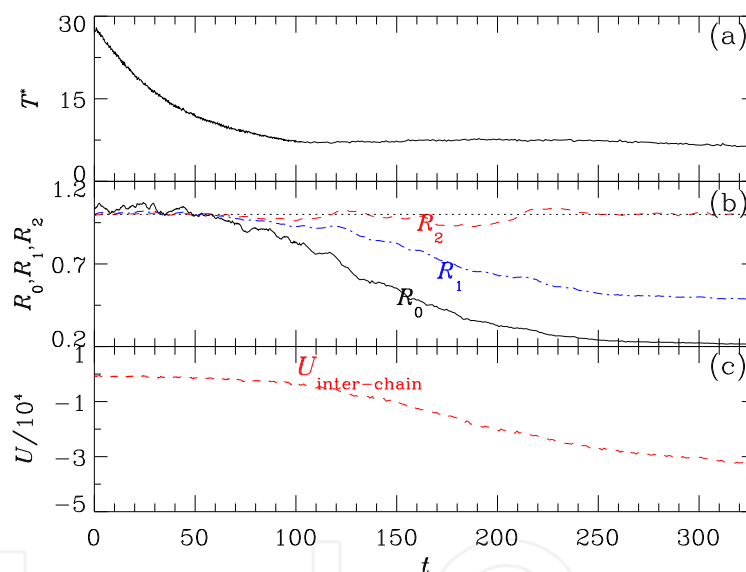

Fig. 13. Same as Fig. 12 for a simulated system with rigidly bonded homogeneous chains ($k_{nn} = \infty$) of length $n = 25$ each (adapted from Ref. [7]).

The typical time evolution of such processes is shown in Fig. 15, for system IV-4. We observe that the values of the parameter R_0 fluctuate in the larger amplitude as compared with those for R_1 and R_2, indicating the occurrence of local alignment between chains fails to survive for triggering the formation of stable structures. In lowering the temperature, the fluctuations change to have the larger amplitude and the longer periods, which seems closer to a stage with monotonic decaying R_0. Entering the regime of $T_P^* \approx 7$, the stronger tendency of alignment between chains signalled by the larger decaying in the value of R_0 still fails to prevent the reverting of the trend, that the enhanced changes in R_0 can only stay with the status as the (larger amplitude) fluctuations. The local mechanical conflicts caused by the angle potentials hinder the pile-up of the packed local segments to form stable higher order structures. We
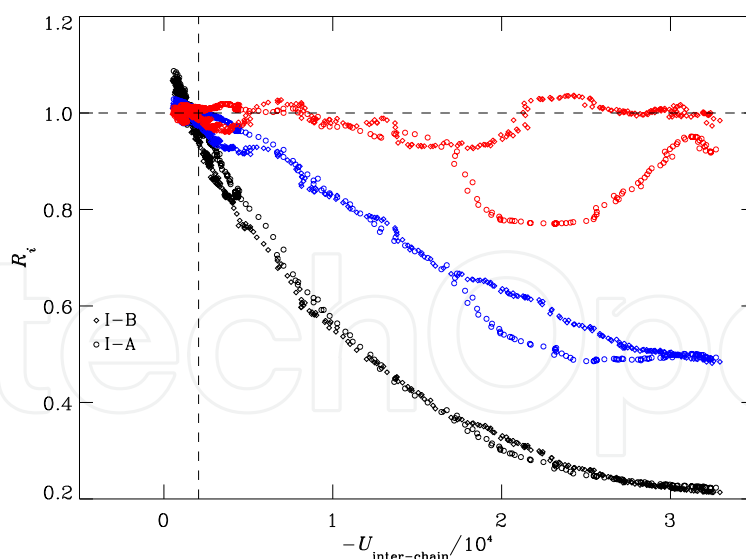
Fig. 14. Same as Fig. 3 for systems with chains of lengths $n = 50$ (circle) and $n = 25$ (diamond), respectively.
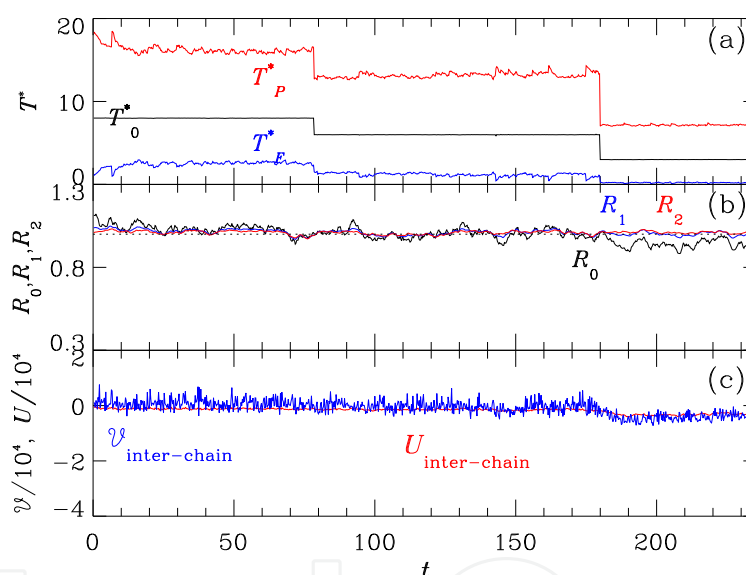

Fig. 15. (Color online) Same as Fig. 4, for the mixed system of polymer and fluid, system IV-4, where $K_b = K_t = 0.1$. (adapted from Ref. [6]).)

conclude that the values of K_b and K_t have to be small for the presence of aggregation process for the polymer chains.

5. Perspectives

The study of aggregations of peptides or proteins and their roles in the occurrence of neurodegenerative diseases, such as Alzheimer's disease [20–22], and the transmissible Creutzfeldt-Jakob disease [23], has become an important cross-disciplined issue for scientists. The important factors for polymer aggregation problems revealed by our analysis, such as the backbone anisotropy and the chain length are suggestive. The suspected origin of Alzheimer's disease at the molecular level is related to the aggregation of proteins $A\beta_{40}$ and $A\beta_{42}$ [20–22] consisting of 40 and 42 residues, respectively. The chain of $A\beta_{40}$ or $A\beta_{42}$ forms two β-strands

and such β-strands form β-sheets [21, 22]. A scenario that describes their aggregation is to consider each β-sheet as an effective polymer chain and has a small degree of effective backbone anisotropy. Thus such effective polymer chains has the trend to aggregate into parallel-domain conformation. It will be interesting in the future work to include more refined backbone anisotropy [24, 25] and quantify its effect on the aggregation dynamics.

6. Acknowledgement

7. References

[1] T. P. J. Knowles, J. F. Smith, A. Craig, C. M. Dobson and M. E. Welland: *Phys. Rev. Lett.* 96 (2006) 238301.

[2] T. P. J. Knowles, A. W. Fitzpatrick, S. Meehan, H. R. Mott, M. Vendruscolo, C. M. Dobson and M. E. Welland: *Science* 318 (2007)1900.

[3] H. D. Nguyen and C. K. Hall: *Proc. Natl. Acad. Sci.* U. S. A. 101 (2004)16180 .

[4] B. Urbanic, L. Cruz, S. Yun, S. V. Buldyrev, G. Bitan, D. B. Teplow and H. E. Stanley: *Proc. Natl. Acad. Sci.* U. S. A. 101 (2004) 17345.

[5] C. M. Dobson: *Nature* 426 (2003)884.

[6] W. J. Ma and C.-K. Hu: *J. Phys. Soc. Japan* 79 (2010) 100402.

[7] W. J. Ma and C.-K. Hu: *J. Phys. Soc. Japan* 79 (2010) 54001.

[8] R. V. Pappu, X. Wang, A. Vitalis and S. L. Crick: *Arch. Biochem. Biophys.* 469 132 (2008).

[9] M. Doi and S. F. Edwards: *The Theory of Polymer Dynamics* (Oxford University Press, New York, 1986).

[10] R. B. Bird, C. F. Curtiss, R. C. Armstrong and O. Hassager: *Dynamics of Polymer Liquids* Vol.2, 2nd ed. (John Wiley and Sons 1987).

[11] H. C. Andersen: *J. Comput. Phys.* 52, 24 (1983).

[12] J. T. Padding, W. J. Briels: *J. Chem. Phys.* 114 (2001) 8685.

[13] D. Steele: *J. Chem. Soc. Faraday Trans.* 2 81 (1985) 1077.

[14] D. Brown and J. H. R. Clarke: *Comput. Phys. Commun.* 62, (1991) 360.

[15] D. D. Voet and J. G. Voet: *BioChemistry* (John Weily and Sons, 1995) 2nd ed. Chap. 7.

[16] W.-J. Ma and C.-K. Hu: *J. Phys. Soc. Jpn.* 79 (2010) 024005.

[17] W.-J. Ma and C.-K. Hu: *J. Phys. Soc. Jpn.* 79 (2010) 024006.

[18] C. Tsallis: *J. Stat. Phys.* 52 (1988) 479.

[19] L. V. Woodcock: *Chem. Phys. Lett.* 10 (1971) 257.

[20] A. Goate, M. C. Chartierharlin, M. Mullan, J. Brown, F. Crawford, L. Fidani, L. Giuffra, A. Haynes, N. Irving, L. James, R. Mant, P. Newton, K. Rooke, P. Roques, C. Talbot, M. Pericakvance, A. Roses, R. Williamson, M. Rossor, M. Owen and J. Hardy: *Nature* 349 (1991) 704.

[21] A. T. Petkova, Y. Ishii, J. J. Balbach, O. N. Antzutkin, R. D. Leapman, F. Delaglio and R Tycko: *Proc. Natl. Acad. Sci.* USA 99 (2002) 16742.

[22] T. Luhrs, C. Ritter, M. Adrian, D. Riek-Loher, B. Bohrmann, H. Doeli, D. Schubert and R. Riek: *Proc. Natl. Acad. Sci.* USA 102 (2005) 17342.

[23] N. J. Cobb, F. D. Sonnichsen, H. Mchaourab and W. K. Surewicz: *Proc. Natl. Acad. Sci.* USA 104 (2007) 18946.

[24] R. Pellarin and A. Caflisch: *J. Mol. Biol.* 360 (2006) 882.

[25] N. Y. Chen, Z. Y. Su, and C. Y. Mou: *Phys. Rev. Lett.* 96 (2006) 078103.
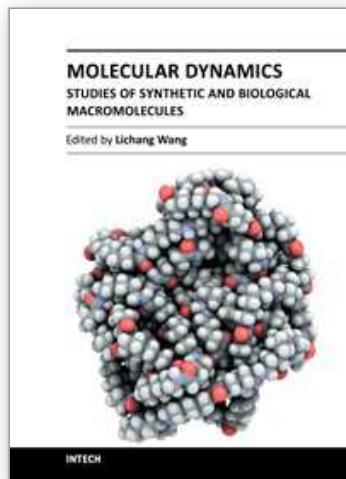
Molecular Dynamics - Studies of Synthetic and Biological Macromolecules

Edited by Prof. Lichang Wang

Molecular Dynamics is a two-volume compendium of the ever-growing applications of molecular dynamics simulations to solve a wider range of scientific and engineering challenges. The contents illustrate the rapid progress on molecular dynamics simulations in many fields of science and technology, such as nanotechnology, energy research, and biology, due to the advances of new dynamics theories and the extraordinary power of today's computers. This second book begins with an introduction of molecular dynamics simulations to macromolecules and then illustrates the computer experiments using molecular dynamics simulations in the studies of synthetic and biological macromolecules, plasmas, and nanomachines. Coverage of this book includes: Complex formation and dynamics of polymers Dynamics of lipid bilayers, peptides, DNA, RNA, and proteins Complex liquids and plasmas Dynamics of molecules on surfaces Nanofluidics and nanomachines

How to reference

In order to correctly reference this scholarly work, feel free to copy and paste the following:

Wen-Jong Ma and Chin-Kun Hu (2012). Backbone Connectivity and Collective Aggregation Phenomena in Polymer Systems, Molecular Dynamics - Studies of Synthetic and Biological Macromolecules, Prof. Lichang Wang (Ed.), ISBN: 978-953-51-0444-5, InTech, Available from: http://www.intechopen.com/books/molecular-dynamics-studies-of-synthetic-and-biological-macromolecules/backbone-connectivity-and-collective-aggregation-phenomena-in-polymer-systems

INTECH

open science | open minds